Segmentation-free Super-resolved 4D FLox MRI Reconstruction Exploiting Navier-Stokes Equations and Spatial Regularization

Sébastien Levilly, Saïd Moussaoui, Jean-Michel Serfaty

SEGMENTATION-FREE SUPER-RESOLVED 4D FLOW MRI RECONSTRUCTION EXPLOITING NAVIER-STOKES EQUATIONS AND SPATIAL REGULARIZATION

Sébastien LEVILLY[⋆†] *Saïd MOUSSAOUI*[†] *Jean-Michel SERFATY*[⋆]

[⋆] Nantes Université, CHU Nantes, CNRS, INSERM, Institut du Thorax, 44000 Nantes, France
[†] Nantes Université, École Centrale Nantes, CNRS, LS2N, 44321 Nantes Cedex 3, France

ABSTRACT

Interest in 4D blood flow MRI grows due to its ability to image the anatomic shape and the three velocity components within a volume along the cardiac cycle. However, some biomarkers' quantification from these data can be inaccurate due to the low resolution of the images. The reference method to improve the spatial resolution numerically is to run computational fluid dynamic (CFD) simulations in order to deduce the associated images in a higher resolution grid. However, such approaches induce complex time-consuming steps and require precise estimates of the vessel wall and the inlet velocity. In this work, an original segmentation-free super-resolution (SR) solution is proposed using an inverse problem resolution approach by the minimization of a compound criterion involving three terms, a mechanical term based on Navier-Stokes equations, and a velocity smoothness promoting term, and a spatially weighted data fidelity term. The proposed solution has been validated regarding estimation error and computation time on simulated data and experimental acquisition from a phantom. Super-resolved velocity reconstruction demonstrates promising performance, even without segmentation knowledge, compared to state-of-the-art solutions.

***Index Terms*—** 4D Flow MRI, super-resolution, inverse problems, segmentation-free, spatial regularization

1. INTRODUCTION

Flow observations in clinical cardiovascular imaging routine are mainly done with 2D Phase-Contrast MRI. 4D flow MRI [1], which measures the anatomy and the three velocity components within a 3D volume and along the cardiac cycle, constitutes a promising tool for clinicians. Unfortunately, the reconstructed image has a limited spatial resolution [1, 2] due to the need to make a trade-off between the signal-to-noise ratio and the acquisition time. Therefore, interpretation along with biomarkers' quantification turn into a complex problem as demonstrated for the wall shear stress [3, 4]. Indeed, low resolution acquisitions imply a coarse estimation of spatial derivatives and implicitly degrade the vessel wall localization. Consequently, the low image resolution is the major source of errors impacting all velocity dependent biomarkers'.

Nowadays, Computation Fluid Dynamics (CFD) simulation is considered as the reference solution to quantify such biomarkers thanks to its fluid mechanics conformity [5]. In fact, it allows to improve numerically the spatial resolution by exploiting the measured data in CFD simulations performed on a finer sampling mesh. These simulations rely on non-linear model based on Navier-Stokes equations whose resolution requires a precise definition of the vessel wall and inlet/outlet velocity fields. Outside of phantom applications [6], CFD simulation and 4D flow MRI matching is complex and a non-applicable task in the clinical routine. To manage this issue, previous contributions proposed machine learning strategies embedding CFD simulation datasets [7, 8], or used directly Navier-Stokes equations with computer vision approaches [9, 10] or adopted inverse problem solutions [11, 12, 13, 14]. In the latter category, some data assimilation methods minimize a data fidelity term under the constraint of Navier-Stokes equations applied within a pre-established segmentation [12, 13], which results in an iterative estimation of the optimal inflow, and then multiple CFD simulations. Rispoli *et al.* [11] proposed to embed the data within a CFD solver called SIMPLER by the minimization of a quadratic optimization problem with a data fidelity term and a fluid mechanic term for convection-diffusion. Unfortunately, the mass conservation equation is set as a hard constraint which requires a Poisson equation resolution for the pressure estimation. Besides, super-resolution (SR) algorithms mainly rely on Navier-Stokes equations solving within a pre-defined fluid domain. The strict respect of fluid mechanics and the precise vessel wall definition requires long computing time and expertise which limits SR applicability in clinical routine.

We proposed in [15], an efficient SR algorithm relying on the inverse problem resolution methodology [16]. A L_2-penalized formulation is used for convection-diffusion and mass conservation instead of applying hard constraints. An extension of this approach is proposed here in such way to improve the segmentation-free velocity reconstruction. In that respect, the optimized criterion, detailed in section 2, is made

This work has been funded by Philips company through the GIE grant.

of three parts: a spatially weighted data fidelity term, a penalization term based on Navier-Stokes equations and a weighted spatial smoothing term applied to the velocity so as to enclose potential fluid areas. Section 3 presents 2D sections of synthetic data and experimental 4D flow MRI measurements on a phantom [17]. In section 4, SR reconstructions are evaluated in terms of root-mean-square error of the velocity vector in the fluid domain and the computation time, especially in comparison to Rispoli *et al.* [11] solution and to our previous contribution [15].

2. METHODS

Let's denote the estimated super-resolved vector by $\mathcal{X} = (\boldsymbol{u}^{\mathrm{t}}, \boldsymbol{v}^{\mathrm{t}}, \boldsymbol{w}^{\mathrm{t}}, \boldsymbol{p}^{\mathrm{t}})^{\mathrm{t}}$ where the velocities components $\boldsymbol{u}$, $\boldsymbol{v}$, $\boldsymbol{w}$ and the pressure field $\boldsymbol{p}$ are organized in the lexicographic order. The proposed super-resolution solution relies on solving the non-linear optimization problem:

$$\hat{\mathcal{X}} = \underset{\mathcal{X} \in \mathrm{R}^N}{\arg\min}\, \mathcal{F}(\mathcal{X}, \mathcal{Y}) + \alpha\, \mathcal{NS}(\mathcal{X}) + \beta\, \mathcal{R}(\mathcal{X}) \qquad (1)$$

where N is the unknown vector size, $\mathcal{F}$ is the data fidelity term, $\mathcal{NS}$ is a regularization term based on the Navier-Stokes equations, and $\mathcal{R}$ is a velocity smoothing term.

The data fidelity term uses a weighted least-squares criterion:

$$\mathcal{F}(\mathcal{X}, \mathcal{Y}) = \|\mathcal{Y} - \mathbf{H}\mathcal{X}\|^2_{\mathbf{W}} \qquad (2)$$

where $\mathcal{Y} = (\boldsymbol{u}_{\mathrm{d}}^{\mathrm{t}}, \boldsymbol{v}_{\mathrm{d}}^{\mathrm{t}}, \boldsymbol{w}_{\mathrm{d}}^{\mathrm{t}})^{\mathrm{t}}$ is a vector containing the data velocity components $\boldsymbol{u}_{\mathrm{d}}$, $\boldsymbol{v}_{\mathrm{d}}$ and $\boldsymbol{w}_{\mathrm{d}}$ stacked in the lexicographic order, $\mathbf{W}$ is a diagonal weight matrix of *a priori* velocity variances [2], and $\mathbf{H}$ is the downsampling and filtering operator [11, 12, 14]. For the sake of simplicity, the 4D flow MRI point spread function (PSF) corresponding to the downsampling process is modeled by a mean filter. Besides, 4D flow MRI phase measurements errors are not identically distributed and the spatially variant standard deviation [2] can be written:

$$\sigma_{v,i} = \frac{\sqrt{2}}{\pi} \frac{V_{\mathrm{enc}}}{\mathrm{SNR}_i} \qquad (3)$$

where V_{enc} is the encoding velocity, and SNR_i the signal-to-noise ratio of the anatomical signal in the i-th voxel. Consequently, the weight matrix, $\mathbf{W} = \mathrm{diag}\left\{\frac{1}{2\sigma^2_{\mathrm{v}\,i}}\right\}_{i=1\cdots N_{\mathrm{d}}}$ where N_{d} is the data size, reduces the data impact outside the potential fluid region of interest.

Blood is regularly assumed to be incompressible [5, 6] and thus to have a constant fluid density ρ and dynamic viscosity μ. In such flows, the fluid velocity $\vec{v} = (u, v, w)^{\mathrm{t}}$ is governed by the mass and momentum conservation equations, also called the incompressible Navier-Stokes equations:

$$\mathrm{div}(\vec{v}) = 0 \qquad (4)$$

$$\rho\, \overline{\overline{\mathrm{grad}}}(\vec{v}) \cdot \vec{v} - \mu\, \Delta\vec{v} + \overline{\mathrm{grad}}\, p = \vec{0} \qquad (5)$$

where p denotes the pressure. Body forces and transient velocity terms are considered negligible in both application cases. The Navier-Stokes equations are applied on the whole field-of-view (FOV) and Dirichlet conditions are used on its borders, in which interpolated velocity is applied on the inlet and the outlet while the no-slip condition is enforced on the other walls. Finite-volume method is generally used to discretize fluid mechanics problems [11, 18, 6], and especially to obtain a first order approximation. Akin to previous contributions [12, 18], a velocity-pressure coupling formulation enables the direct computation of all velocity components which differ from a segregated algorithm used in Rispoli *et al.* [11] solution. Thus, the regularization term $\mathcal{NS}(\mathcal{X})$, based on equations (4) and (5), is linearized in the vicinity of any $\mathcal{X}_k$ such as the quadratic norm of the fluid mechanic equations becomes:

$$\mathcal{NS}_k(\mathcal{X}) = \|\mathbf{S}_{\mathcal{X}_k}\mathcal{X} - \boldsymbol{b}\|^2_2 \qquad (6)$$

where $\mathbf{S}_{\mathcal{X}_k}$ is the convection-diffusion matrix computed from $\mathcal{X}_k$ and $\boldsymbol{b}$ contains the boundary conditions.

Further investigations revealed the importance of segmentation guidance at the risk of fluid domain velocities estimation being degraded by the ones outside this domain, especially close to the vessel wall. In order to limit outer velocities impact, the regularization term $\mathcal{R}$ relies on weighted spatial smoothing applied on each velocity components, and is defined as:

$$\mathcal{R}(\mathcal{X}) = \|\mathbf{G}_{\mathrm{x}}\mathcal{X}\|^2_{\overline{\mathbf{W}}} + \|\mathbf{G}_{\mathrm{y}}\mathcal{X}\|^2_{\overline{\mathbf{W}}} + \|\mathbf{G}_{\mathrm{z}}\mathcal{X}\|^2_{\overline{\mathbf{W}}} = \mathcal{X}^{\mathrm{t}}\mathbf{M}\mathcal{X} \qquad (7)$$

with $\mathbf{M} = \mathbf{G}_{\mathrm{x}}^{\mathrm{t}}\overline{\mathbf{W}}\mathbf{G}_{\mathrm{x}} + \mathbf{G}_{\mathrm{y}}^{\mathrm{t}}\overline{\mathbf{W}}\mathbf{G}_{\mathrm{y}} + \mathbf{G}_{\mathrm{z}}^{\mathrm{t}}\overline{\mathbf{W}}\mathbf{G}_{\mathrm{z}}$ where $\mathbf{G}_{\mathrm{x}}$, $\mathbf{G}_{\mathrm{y}}$ and $\mathbf{G}_{\mathrm{z}}$ are the spatial derivative matrices, and $\overline{\mathbf{W}}$ is a diagonal matrix filled with the *a priori* variances. The standard deviation is computed from the linearly interpolated magnetization and equation (3). Thus, outer velocities are significantly smoothed while the fluid domain velocities are mainly regularized by Navier-Stokes equations and softened to a lesser extent by $\mathcal{R}(\mathcal{X})$.

The non-linear optimization problem (1) is solved by dealing with the following weighted least-squares minimization problem for successive $\mathcal{X}_k$:

$$\min_{\mathcal{X} \in \mathrm{R}^N} \|\mathcal{Y} - \mathbf{H}\mathcal{X}\|^2_{\mathbf{W}} + \alpha\, \|\mathbf{S}_{\mathcal{X}_k}\mathcal{X} - \boldsymbol{b}\|^2_2 + \beta\, \mathcal{X}^{\mathrm{t}}\mathbf{M}\mathcal{X} \qquad (8)$$

whose solution $\hat{\mathcal{X}}$ is obtained by solving the following linear system:

$$\left(\mathbf{H}^{\mathrm{t}}\mathbf{W}\mathbf{H} + \alpha\, \mathbf{S}^{\mathrm{t}}_{\mathcal{X}_k}\mathbf{S}_{\mathcal{X}_k} + \beta\, \mathbf{M}\right)\mathcal{X} = \left(\mathbf{H}^{\mathrm{t}}\mathbf{W}\mathcal{Y} + \alpha\, \mathbf{S}^{\mathrm{t}}_{\mathcal{X}_k}\boldsymbol{b}\right) \qquad (9)$$

using a preconditioned linear conjugate gradient algorithm. This iterative scheme efficiency is also the result of the construction of dedicated operators instead of large sparse matrices for $\mathbf{H}$, $\mathbf{S}_{\mathcal{X}_k}$, $\mathbf{M}$ and $\mathbf{W}$. The algorithm is assumed to be converged once the normalized solution difference between two iterations reaches a tolerance threshold (10^{-6}). This non-linear optimization solving is summarized in the Algorithm 1.

Algorithm 1: SFSR Algorithm

Data: $\mathcal{Y} \leftarrow (\boldsymbol{u}_{\mathrm{d}}^{\mathrm{t}}, \boldsymbol{v}_{\mathrm{d}}^{\mathrm{t}}, \boldsymbol{w}_{\mathrm{d}}^{\mathrm{t}})^{\mathrm{t}}$
Result: $\hat{\mathcal{X}} \leftarrow (\hat{\boldsymbol{u}}^{\mathrm{t}}, \hat{\boldsymbol{v}}^{\mathrm{t}}, \hat{\boldsymbol{w}}^{\mathrm{t}}, \hat{\boldsymbol{p}}^{\mathrm{t}})^{\mathrm{t}}$
$\mathbf{W}$ is computed with equation (3) ;
$\boldsymbol{b}$ contains the velocity domain information ;
$k \leftarrow 1$; $\varepsilon \leftarrow 1$; $k_{\max} \leftarrow 100$; $tol \leftarrow 10^{-6}$;
$\mathcal{X}_0 \leftarrow$ 4D flow MRI velocity linear interpolation ;
while $k \leq k_{max}$ *and* $\varepsilon \geq tol$ **do**
  Convection-diffusion matrix $\mathbf{S}_{\mathcal{X}_{k-1}}$ computation ;
  Linear problem (9) solving with a tolerance of 10^{-5} and 1000 as maximum of iteration ;
  $\varepsilon \leftarrow \|\hat{\mathcal{X}}_k - \hat{\mathcal{X}}_{k-1}\|_2^2 / \|\hat{\mathcal{X}}_{k-1}\|_2^2$;
  $k \leftarrow k + 1$
end

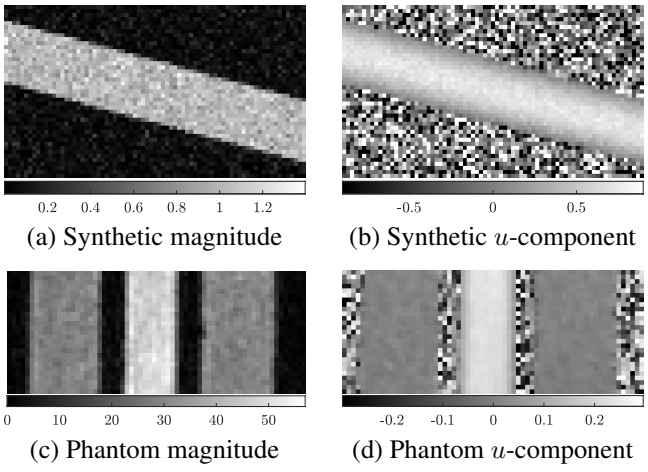

(a) Synthetic magnitude (b) Synthetic u-component
(c) Phantom magnitude (d) Phantom u-component

Fig. 1. Synthetic and Phantom datasets (velocity in $\mathrm{m/s}$).

3. VALIDATION

The proposed solution, called segmentation-free-SR (SFSR), has been validated on a 2D synthetic dataset and a 2D section of 4D flow MRI acquisition [17]. Figure 1 illustrates the magnetization and u-component of these 2D datasets. The synthetic dataset FOV is set to $15 \times 8.63\ \mathrm{cm}^2$ and divided on two regions: a non-fluid area with a low magnetization in opposition to an other area of fluid circulation. The latter is defined as a straight tilted cylinder with a radius of $1.5\ \mathrm{cm}$ leading to a parabolic velocity field, called Poiseuille in non-pulsatile flow, and with a maximum of $0.75\ \mathrm{m/s}$. The fluid model uses a dynamic viscosity μ of $0.0032\ \mathrm{Pa.s}$ and a fluid density ρ of $1060\ \mathrm{Kg/m^3}$. The synthetic 4D flow MRI dataset is obtained by computing the Poiseuille flow on a thinner grid set to an isotropic (ISO) spatial resolution of $1\ \mathrm{mm}$. The latter is then filtered with a 2×2 mean kernel introducing partial volume effect and leading to a spatial resolution of $2\ \mathrm{mm}$. Finally, a spatially variant zero-mean Gaussian noise is added to the filtered velocity with a σ_{v} conform to equation (3) and the filtered magnetization. This standard deviation is set to $5\,\%$ of the V_{enc} in the fluid domain and limited by the V_{enc}, which is defined as $120\,\%$ of the maximum theoretical velocity.

The phantom 4D flow MRI dataset used in this study relies on the steady case presented in [17]. The fluid flows through a straight square pipe with a section of $25 \times 25\ \mathrm{mm}^2$. An MRI-compatible gear pump (CardioFlow 5000, Shelley Medical Technology) maintains a steady flow of $98.7\ \mathrm{mL/s}$ reaching a maximal velocity of $28\ \mathrm{cm/s}$. Only a 2D section of the acquired dataset, placed along the pipe axis, was used with a spatial resolution of $2.2 \times 2.2\ \mathrm{mm}^2$. The reference velocity field has been computed by CFD simulation (Star CCM+, Siemens), with a finite-volume method on a Cartesian mesh of 1,725,000 $0.5\ \mathrm{mm}$-size cubic elements [17].

The proposed approach SFSR, Rispoli *et al.* [11] named SbSR for SIMPLER based-SR, and the previous solution [15] called Penalized-SR (PSR) are evaluated in terms of Root-Mean-Square Error (RMSE) and computation time (CT). The SR estimation is compared to the corresponding theoretical or numerical reference velocity field. The RMSE, restricted to the fluid domain, is defined as the percentage of the data noise level such as:

$$\mathrm{RMSE}(\boldsymbol{r}) = {}^{1}/_{\mathrm{RMSE_d}} \times \sqrt{{}^{\Sigma_{i=1}^{N}(\boldsymbol{r}_i - \overline{\boldsymbol{r}}_i)^2}/_{N}} \qquad (10)$$

where $\overline{\boldsymbol{r}}$ contains the super-resolved reference velocity field, $\mathrm{RMSE_d}$ is equal to $\sqrt{\frac{1}{N_{\mathrm{d}}} \sum_{i=1}^{N_{\mathrm{d}}} \left(\mathcal{Y}_i - \overline{\mathcal{Y}}_i\right)^2}$, and $\overline{\mathcal{Y}}$ is for the low resolution unfiltered reference velocity field.

4. RESULTS & DISCUSSION

The evaluation of the SR algorithms, SFSR and SbSR, have been done on the synthetic and phantom datasets illustrated in Fig. 1. Optimal regularization parameters, α and β, are set such as they minimize the RMSE on their associated datasets as depicted by Fig. 2(a) and Fig. 2(b). One can observe in Fig. 2(c) the problem (1) criterion minimization on both datasets with their optimal set of parameters. The resulting SR velocity grids are shown in Fig. 3 for both datasets and algorithms. Regions are distinctly observable on each dataset and method.

	Synthetic dataset		Phantom dataset	
	RMSE [%]	CT [s]	RMSE [%]	CT [s]
SFSR	35.2	34	53.9	21
PSR	30.3	14	39.2	7
PSR*	44.2-55.9	813	72.6-93.3	482
SbSR	59.9	437	89.2	205

Table 1. Performance indicators in application to the synthetic and phantom datasets.

In terms of performance, Table 1 presents the RMSE and CT of the SR solutions by a factor 2 by dimension on both

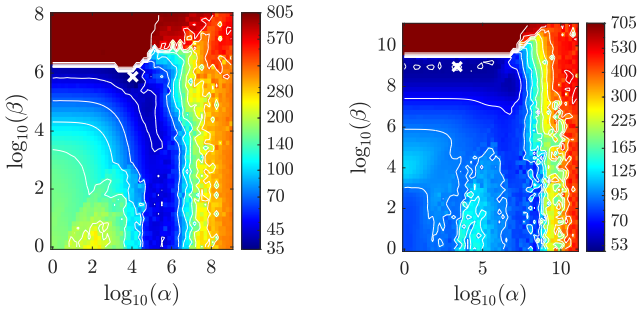

(a) SFSR RMSE on the synthetic dataset

(b) SFSR RMSE on the phantom dataset

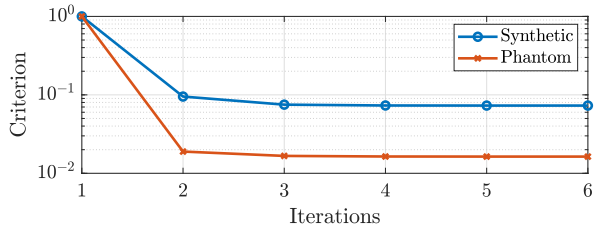

(c) SFSR Criterion on both datasets

Fig. 2. SFSR hyper-parameters and criterion optimization on both datasets.

synthetic and phantom datasets. SFSR presents a RMSE 60 % smaller than the SbSR one for each dataset while PSR RMSE is even smaller. PSR solution exploits the segmentation meanwhile PSR* problem is equivalent to the SFSR approach with $\beta = 0$. SFSR solution clearly benefits from smoothing term in comparison with the unstable results of PSR*. Observation of 2D error maps, in Fig. 4, revealed that the quantification error is significantly higher in the vicinity of the inlet and outlet of the FOV for SbSR in contrast to SFSR solution. Then, SbSR has interesting performance in the center of the FOV while SFSR is more uniform in term of quantification. Besides, SbSR presents higher error magnitudes which lie mostly on the fluid domain borders as observed in Fig. 4(a) and Fig. 4(c). Although SFSR estimation is less precise outside the fluid domain, its impact on the inner velocities remains admissible. The implementation has been done on MATLAB (R2021b) on a workstation with an Intel Core i9-11950H (2.60GHz) and 64Gb of RAM. SFSR algorithm is 10 times faster than the SbSR solution on both datasets. SbSR performance is mainly limited due to the divergence-free constraint and its Poisson equation solving in comparison with the penalized formulation of PSR and SFSR.

Despite the promising quantification performance, SFSR presents residual error mostly close to the vessel wall which are proned to degrade wall-related biomarkers. That error might be induced by a velocity plateau outside the fluid domain (see Fig. 4(d)). Consequently, perspectives concern the use of a sparsity promoting term or adding a L_2-norm on velocity components to pull outer velocities close to zero.

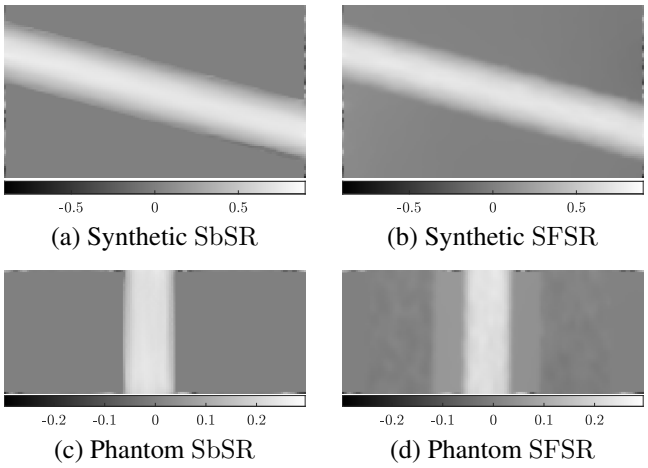

(a) Synthetic SbSR

(b) Synthetic SFSR

(c) Phantom SbSR

(d) Phantom SFSR

Fig. 3. Super-resolved velocity u-component $[\mathrm{m/s}]$.

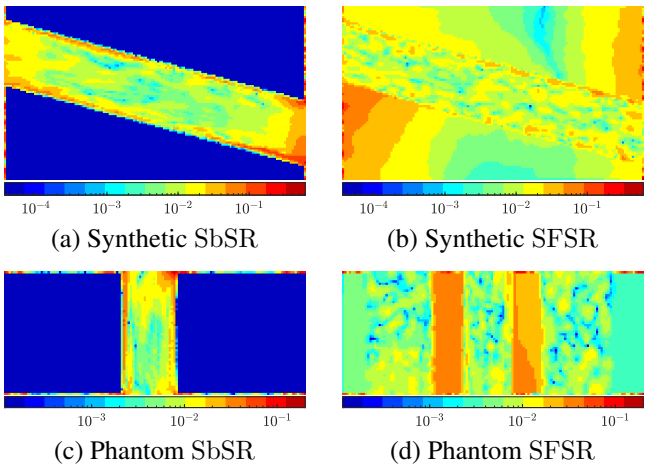

(a) Synthetic SbSR

(b) Synthetic SFSR

(c) Phantom SbSR

(d) Phantom SFSR

Fig. 4. Error norm of the super-resolved vectors $[\mathrm{m/s}]$.

5. CONCLUSION

This paper introduced a new segmentation-free algorithm to compute efficiently a super-resolved solution of velocity vectors from 4D flow MRI data. The proposed SFSR solution, based on inverse problem theory, relies on two additional prior: one term using the Navier-Stokes equations ensuring realistic fluid flow reconstruction and one term smoothing the velocity outside the potential fluid domain enabling a reliable segmentation-free approach. Using penalization in contrast to hard constraint on the Navier-Stokes equations provides a computationally efficient solution which is also demonstrated by satisfying RMSE performance.

Future investigations will be conducted on datasets over the cardiac cycle in order to observe the pulsatile effect on the proposed solution.

6. REFERENCES

[1] M. Markl, A. Frydrychowicz, S. Kozerke, M. Hope, and O. Wieben, "4D Flow MRI," *J. Magn. Reson. Imaging*, vol. 36, no. 5, pp. 1015–1036, 2012.

[2] N. J. Pelc, M. A. Bernstein, A. Shimakawa, and G. H. Glover, "Encoding strategies for three-direction phase-contrast MR imaging of flow," *J. Magn. Reson. Imaging*, vol. 1, no. 4, pp. 405–413, 1991.

[3] A. F. Stalder, M. F. Russe, A. Frydrychowicz, J. Bock, J. Hennig, and M. Markl, "Quantitative 2D and 3D phase contrast MRI: Optimized analysis of blood flow and vessel wall parameters," *Mag. Reson. Med.*, vol. 60, no. 5, pp. 1218–1231, 2008.

[4] S. Levilly, M. Castagna, J. Idier, F. Bonnefoy, D. Le Touzé, S. Moussaoui, P. Paul-Gilloteaux, and J.-M. Serfaty, "Towards quantitative evaluation of wall shear stress from 4D flow imaging," *Magn. Reson. Imaging*, vol. 74, pp. 232–243, 2020.

[5] L. Boussel, V. L. Rayz, A. Martin, G. Acevedo-Bolton, M. T. Lawton, R. Higashida, W. S. Smith, W. L. Young, and D. Saloner, "Phase-contrast magnetic resonance imaging measurements in intracranial aneurysms in vivo of flow patterns, velocity fields, and wall shear stress: comparison with computational fluid dynamics.," *Mag. Reson. Med.*, vol. 61, pp. 409–417, 02 2009.

[6] T. Puiseux, A. Sewonu, O. Meyrignac, H. Rousseau, F. Nicoud, S. Mendez, and R. Moreno, "Reconciling PC-MRI and CFD: An in-vitro study," *NMR Biomed*, vol. 32, no. 5, pp. e4063, 2019.

[7] F. Gaidzik, D. Stucht, C. Roloff, O. Speck, D. Thévenin, and G. Janiga, "Transient flow prediction in an idealized aneurysm geometry using data assimilation," *Comput. Biol. Med.*, vol. 115, 2019.

[8] I. Perez-Raya, M. F. Fathi, A. Baghaie, R. H. Sacho, K. M. Koch, and R. M. D'Souza, "Towards multi-modal data fusion for super-resolution and denoising of 4D-flow MRI," *Int. J. Numer. Meth. Bio.*, vol. 36, no. 9, 2020.

[9] N. de Hoon, R. van Pelt, A. Jalba, and A. Vilanova, "4D MRI flow coupled to physics-based fluid simulation for blood-flow visualization," *Comput. Graph. Forum*, vol. 33, no. 3, pp. 121–130, 2014.

[10] F. M. Callaghan and S. M. Grieve, "Spatial resolution and velocity field improvement of 4D-flow MRI," *Mag. Reson. Med.*, vol. 78, no. 5, pp. 1959–1968, 2017.

[11] V. C. Rispoli, J. F. Nielsen, K. S. Nayak, and J. LA Carvalho, "Computational fluid dynamics simulations of blood flow regularized by 3D phase contrast MRI," *Biomed. Eng. Online*, vol. 14, no. 1, pp. 110, 2015.

[12] M. D'Elia, M. Perego, and A. Veneziani, "A variational data assimilation procedure for the incompressible Navier-Stokes equations in hemodynamics," *J. Sci. Comput.*, vol. 52, no. 2, pp. 340–359, 2012.

[13] S. W. Funke, M. Nordaas, Ø. Evju, M. S. Alnæs, and K. A. Mardal, "Variational data assimilation for transient blood flow simulations: Cerebral aneurysms as an illustrative example," *Int. J. Numer. Meth. Bio.*, vol. 35, no. 1, 2019.

[14] M. F. Fathi, I. Perez-Raya, A. Baghaie, P. Berg, G. Janiga, A. Arzani, and R. M. D'Souza, "Super-resolution and denoising of 4D-flow MRI using physics-informed deep neural nets," *Comput. Meth. Prog. Bio.*, p. 105729, 2020.

[15] S. Levilly, S. Moussaoui, and J.-M. Serfaty, "Navier-stokes-based regularization for 4D flow MRI super-resolution," in *Proc. IEEE 19th I. S. Biomed. Imaging (ISBI)*, 2022.

[16] J. Idier, *Bayesian Approach to Inverse Problems*, ISTE Ltd and John Wiley & Sons Inc, Apr. 2008.

[17] M. Castagna, S. Levilly, P. Paul-Gilloteaux, S. Moussaoui, J. Rousset, F. Bonnefoy, J. Idier, J.-M. Serfaty, and D. Le Touzé, "An LDV based method to quantify the error of PC-MRI derived wall shear stress measurement," *Sci. Rep.*, vol. 11, 2021.

[18] Z. Mazhar, *Fully Implicit, Coupled Procedures in Computational Fluid Dynamics*, vol. 115, Springer, Cham, 2016.